IUTAM Symposium on the Dynamics of Extreme Events Influenced by Climate Change (2013)

Effects of water seepage on the stability of soil-slopes

Q.Q. Liu*, J.C. Li

Laboratory for Mechanics in Fluid Solid Coupling System, Institute of Mechanics, Chinese Academy of Sciences, Beijing 100190, China

Abstract

Landslide is a kind of severe natural disaster and societal hazard throughout the world. Among various effecting factors, water is commonly known as one of the major triggers for landslide failures. In this paper, a coupling model of water-seepage and stability analysis has been developed for analyzing the effect of water on the stability of slopes. A combination of spline curves and genetic algorithm is used to locate the critical slip surface for slope stability calculations. A new analytical solution of the linearized Boussinesq equation was developed for one-dimensional groundwater flow in unconfined aquifer. An actual landslide located in the Three Gorges Reservoir was analyzed by simulating the changes of the seepage field caused by rainfall and water level fluctuation. The influences of water seepage on the stability of landslide were discussed with emphasis. The results show that rainfall infiltration and the variation of water level can tremendously influence the stability of slopes.

Keywords: landslide, stability of landslide, water seepage, rainfall, fluctuation of reservoir water level

1. Introduction

Landslides, as one of the natural disasters occurring all of a sudden, commonly cause severe damage, thus constituting a severe threat to human being's life and property. According to statistics, from 1996-2000, landslides caused over 20 billions Yuan in damage and over 900 people deaths in China every year. In general, the occurring of a landslide is mainly related to bedrock geology, geotechnical properties, rainfall, groundwater conditions and land-use conditions. Among them, water is commonly known as one of the major triggers for landslide failures. According to statistics, over 90% landslide failures were related to water. Especially, climate change will result in more frequent and intensive storm events, and the landslide disasters become increasingly more severe. However, the influence of water on slope stability is very complex. In general, the effects of water may manifest itself in many ways, such as soil suction reduction, pore pressure growth, water table lifting, soil unit weight rising, as well as anti-

---

* Corresponding author. Tel.: +86-10-82544202; fax: +86-10-62561284.
  E-mail address: qqliu@imech.ac.cn

shear strength weakening [1-3]. As a result, the interactions of water and earth slope should be investigated and understood in a broader sense.

During the recent decades, there have been extensive investigations on the mechanism of landslide failure caused by water seepage from rainfall or water level fluctuation. Many empirical and semi-empirical relationships have been established to estimate the relationship of rainfall and landslide failure quantitatively. However, most of the empirical researches aiming at a certain specific slope type or region only covered very limited parameter range. Accordingly, there seems to be a shift in emphasis from the empirical approach to the dynamic model to rainfall-induced landslides [4-8]. Some researchers have analyzed the failure of slopes induced by fissure infiltration during rainstorm [9-12]. However comparatively, the dynamic study of interaction mechanism of water seepage and slope stability is still weak relatively. More and more investigations are concerned with the physical mechanism of landslide failure induced by water seepage. Therefore, the objective of the current research is to develop the coupling model of water seepage and slope stability for examining the effect of water seepage on slope stability, which will certainly be helpful for gaining an insight into the mechanism of water-induced landslide failures.

2. Water seepage model in slopes

2.1. Saturated-unsaturated seepage model

All Under the assumption that the air pressure remains constant and the water is incompressible, the governing equation for seepage flows in a slope can be written as following [8]:

$$C(h)\frac{\partial H}{\partial t} = \frac{\partial}{\partial x}\left[K_x(h)\frac{\partial H}{\partial x}\right] + \frac{\partial}{\partial y}\left[K_y(h)\frac{\partial H}{\partial y}\right], \tag{1}$$

where $H = h + y$ is the total hydraulic head; h is the pressure head; y is the elevation head; K_x and K_y are the hydraulic conductivities in the x and y directions, respectively; $C = \partial\theta/\partial h$ is the volumetric water retention capacity, and θ is the volumetric water content.

To solve eq. (1), the Galerkin finite element discretization in space and the finite difference discretization in time are used, and the triangle finite element is adopted. The relationship between the total hydraulic head $H(x,y,t)$ and the nodal hydraulic head $H_i(t)$ is approximately written as

$$H(x,y,t) = \sum_{i=1}^{3} N_i(x,y)H_i(t), \tag{2}$$

where $N_i = (a_i + b_i x + c_i y)/2A$, i = 1, 2, 3; A is the area of triangle element; a_i, b_i, and c_i are given based on the triangle nodal coordinates.

For the total solution domain, the matrix function is

$$\sum_e \iint \left[\frac{\partial N_i}{\partial x} K_x(h)\frac{\partial H}{\partial x} + \frac{\partial N_i}{\partial y} K_y(h)\frac{\partial H}{\partial y} - C(h)\frac{\partial H}{\partial t} N_i\right] \times \mathrm{d}x\mathrm{d}y = 0. \tag{3}$$

Because the relationship between water content and matric suction is highly nonlinear, numerical approximation using C(h) = d/dh generally exhibits very poor preservation of mass balance problems [13]. Consequently, $C(h_i) = (\theta^{t+\Delta t} - \theta^t)/(h^{t+\Delta t} - h^t)$ is used, and mass lumping is employed to improve the numerical stability of the finite element models since previous studies indicated that consistent mass formulation could cause numerical oscillations [14].

For an element *e*, the matrix equation is written as

$$\frac{\overline{K_x}}{4A}\begin{pmatrix} b_ib_i & b_ib_j & b_ib_m \\ b_jb_i & b_jb_j & b_jb_m \\ b_mb_i & b_mb_j & b_mb_m \end{pmatrix}\begin{pmatrix} H_i \\ H_j \\ H_m \end{pmatrix}+\frac{\overline{K_y}}{4A}\begin{pmatrix} c_ic_i & c_ic_j & c_ic_m \\ c_jc_i & c_jc_j & c_jc_m \\ c_mc_i & c_mc_j & c_mc_m \end{pmatrix}\begin{pmatrix} H_i \\ H_j \\ H_m \end{pmatrix}+\frac{A}{3}\begin{pmatrix} C(h_i) & 0 & 0 \\ 0 & C(h_i) & 0 \\ 0 & 0 & C(h_i) \end{pmatrix}\begin{pmatrix} \dfrac{dH_i}{dt} \\ \dfrac{dH_j}{dt} \\ \dfrac{dH_m}{dt} \end{pmatrix}=0 \tag{4}$$

where $\overline{K}=[K(h_i)+K(h_j)+K(h_m)]/3$. Based on eq.(4), the equation including all the nodal points is obtained and simply expressed in the following form:

$$[D]\{H\}+[B]\left\{\frac{dH}{dt}\right\}=0. \tag{5}$$

Introducing a backward finite difference of the time derivative term, the eq. (5) is written as

$$\left[D^{t+\Delta t}+\frac{B^{t+\Delta t}}{\Delta t}\right]\{H^{t+\Delta t}\}=\frac{B^{t+\Delta t}}{\Delta t}\{H^t\}. \tag{6}$$

$[D]$ and $[B]$ are the functions of $H^{t+\Delta t}$, and the iterative scheme is employed to solve eq. (6).

The model was validated by the experiments [15]. The soil belongs to a kind of fine sand with porous rate $n=0.44$ and the saturated hydraulic conductivity $K_{sat}=3.3\times10^3$m/s. The comparison between observation and prediction by the proposed model is shown in Fig. 1. On the whole, the observation and the predicted results in water level exhibit a good agreement.
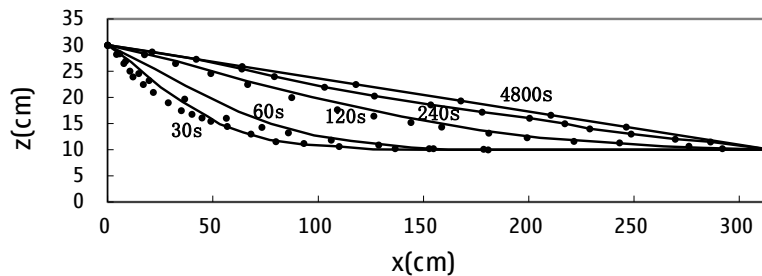
Fig.1. Comparison between the experimental results and numerical results of water level.
(*line* is numerical results , *dot* is experimental results)

2.2. An approximate solution for groundwater table location during reservoir drawdown

As reservoir water is descending, the groundwater table in the adjacent aquifer falls down correspondingly. The prediction of groundwater table variations in the aquifer during reservoir drawdown is an important issue for stability analysis. Generally speaking, the governing equation for one-dimensional, lateral, unconfined groundwater flows is the Boussinesq equation [16] as below:

$$\frac{\partial h}{\partial t}=\frac{K}{n_e}\frac{\partial}{\partial x}(h\frac{\partial h}{\partial x}) \tag{7}$$

in which h= groundwater table height from the impermeable aquifer base; K= hydraulic conductivity; n_e= specific yield; x= horizontal coordinate. Rainfall infiltration is not taken into account. Moreover, the capillary effects on the

groundwater table elevation are neglected as well.

In the meanwhile, the boundary and initial conditions for a semi-infinite aquifer in a slope look like:

$$h[X(t),t] = H_1(t), \quad X(t) = H_1(t)\cot\beta, \qquad t \geq 0, \tag{8}$$

$$h(\infty,t) = h_i \qquad\qquad\qquad\qquad t \geq 0, \tag{9}$$

$$h(x,0) = h_i \qquad\qquad\qquad H_1(0)\cot\beta \leq x < \infty \tag{10}$$

in which $X(t) = x$-coordinate of the moving boundary and the origin of the x-coordinate is located at the toe of the sloped interface; β = slope angle; h_i = initial height of the groundwater table across the aquifer; and $H_1(t)$ = reservoir water level at the left boundary .

In reality, the groundwater flow in the adjacent aquifer may not instantly follow the variation of water surface in the reservoir, thus resulting in the formation of a seepage face on the slope if the reservoir water level drops quickly enough or seepage flows move slowly enough. In the present study, we assume that the exit point happens to be at the water surface of reservoir, namely, the effect of seepage face is neglected for the sake of convenient manipulation. Fig. 2 depicts an idealized cross section of the model under consideration.
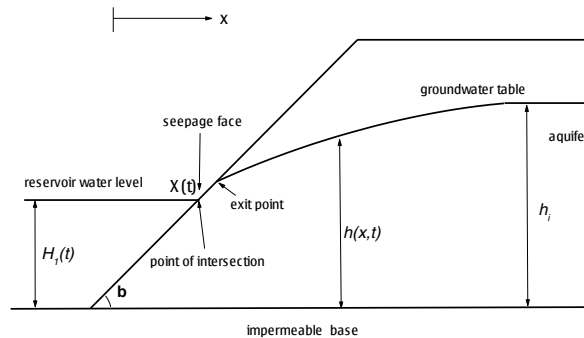
Fig.2. Sketch of idealized cross section for the model

Then, we prefer firstly to consider the drawdown condition at a constant speed, that is, the reservoir water level can be specified as

$$H_1(t) = h_i - Vt \tag{11}$$

in which V is the drawdown speed of reservoir water level. Since $H_1(t)$ is a positive height of reservoir water level, which implies that Vt should always be kept no larger than h_i.

Since the moving boundary condition in the mathematical formulation precludes analytical solutions even for the linearized Boussinesq equation, we have transformed the Boussinesq equation into an advection-diffusion equation to facilitate the solution of this moving boundary problem. Based on the Laplace transformation, we yield an analytical solution of a fixed boundary problem, which is further simplified to upper and lower polynomial solutions for convenient practical use [17].

$$u(z,t) = V\int_0^t (-p+t)z \exp\left(\frac{-V^2 p^2 n_e \cot^2\beta - n_e z^2 + 2Vpn_e z\cot\beta}{4Kh_i p}\right) \bigg/ \left(2\sqrt{\frac{\pi n_e p^3}{Kh_i}}\right) dp \tag{12}$$

$$h(z,t) = h_i - V\int_0^t (-p+t)z \exp\left(\frac{-V^2 p^2 n_e \cot^2\beta - n_e z^2 + 2Vpn_e z\cot\beta}{4Kh_i p}\right) \bigg/ \left(2\sqrt{\frac{\pi n_e p^3}{Kh_i}}\right) dp \tag{13}$$

This analytic solution representing groundwater table variation in the adjacent aquifer during reservoir drawdown looks too complicated to be easily used for practical engineering. For convenient practical use, the analytic solution is further simplified to upper and lower polynomial solutions.

$$h_l(z,t) = h_i - VtM(\lambda)\exp\left[\left(\frac{2Vt\cot\beta}{z}\right)\lambda^2\right] \tag{14}$$

$$h_u(z,t) = h_i - VtM(\lambda)\exp\left[\left(\frac{2z-Vt\cot\beta}{z^2}Vt\cot\beta\right)\lambda^2\right] \tag{15}$$

$$M(\lambda) = \begin{cases} 0.1091\lambda^4 - 0.7501\lambda^3 + 1.9283\lambda^2 - 2.2319\lambda + 1 & 0 \le \lambda < 2 \\ 0 & \lambda \ge 2 \end{cases} \tag{16}$$

The effectiveness of the approximate solution is verified by comparing the upper solution with numerical results. The simulations show that the upper polynomial solution compares reasonably well with the numerical one (Fig. 3).
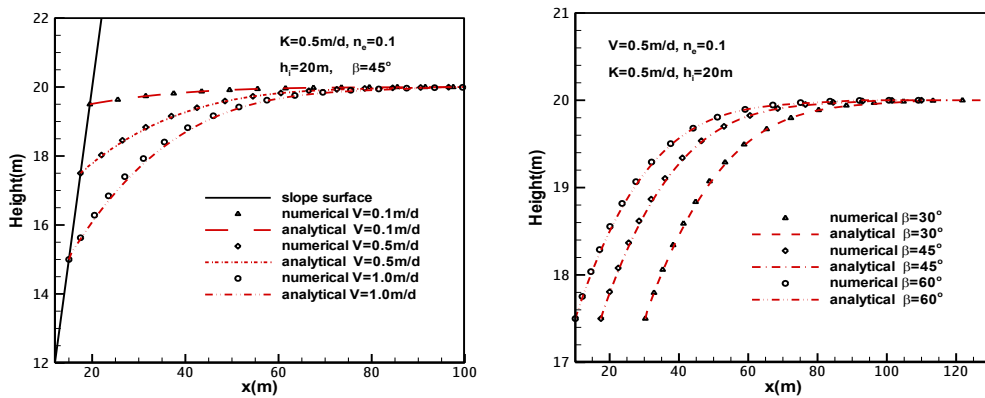
(a) for different drawdown speeds V (b) for different slope angles β

Fig.3. Comparison between upper polynomial solutions and explicit finite-difference solutions

3. Stability analysis model

3.1. Limit Equilibrium Method

The slope stability is commonly analyzed by using the limit equilibrium method of slices. The failing soil mass is divided into a number of vertical slices to calculate the factor of safety, defined as the ratio of the resisting shear strength to the mobilized shear stress to maintain static equilibrium. Both force and moment equilibrium can be satisfied explicitly. Fig. 4 shows the details of inter-slice forces for a typical slice.

The equations of force and momentum equilibrium are respectively written as
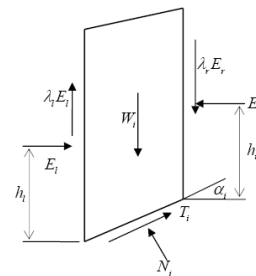
Fig.4. Forces acting on a typical slice

$$E_{r} = \frac{\begin{bmatrix} (W_i - c_i l_i \sin\alpha_i / F + U_i \tan\varphi_i \sin\alpha_i / F)(\tan\varphi_i \cos\alpha_i / F - \sin\alpha_i) \\ -(-c_i l_i \cos\alpha_i / F + U_i \tan\varphi_i \cos\alpha_i / F)(\cos\alpha_i + \tan\varphi_i \sin\alpha_i / F) \\ +E_1(\cos\alpha_i + \tan\varphi_i \sin\alpha_i / F - \lambda_1 \tan\varphi_i \cos\alpha_i / F + \lambda_1 \sin\alpha_i) \end{bmatrix}}{[\cos\alpha_i + \tan\varphi_i \sin\alpha_i / F - \lambda_r \tan\varphi_i \cos\alpha_i / F + \lambda_r \sin\alpha_i]},$$
(17)

$$h_r = \frac{E_1}{E_r}\left(h_1 - \frac{\Delta x}{2}\tan\alpha_i + \lambda_1 \frac{\Delta x}{2}\right) + \frac{W_i}{E_r}(x_G - x_1) + \frac{\Delta x}{2}(\lambda_r - \tan\alpha_i),$$
(18)

where F is the safety factor; E_1 and E_r are the left and the right inter-slice forces, respectively. The total normal force and the pore water pressure on the slice base are N_i and U, respectively. The weight of slice is W_i. The angle between the slice base and the horizontal line is α_i, and λ is the inclination angle of inter-slice force. x_G is x-coordinate of slice center of gravity. x is the slice width.

3.2. Method for searching for critical slip surface

In application of limit equilibrium methods, the identification of the critical slip surface is of principal importance. In this study the spline curve in conjunction with genetic algorithm is used to search the critical slip surface, and Spencer's method is employed to calculate the safety factor [18].
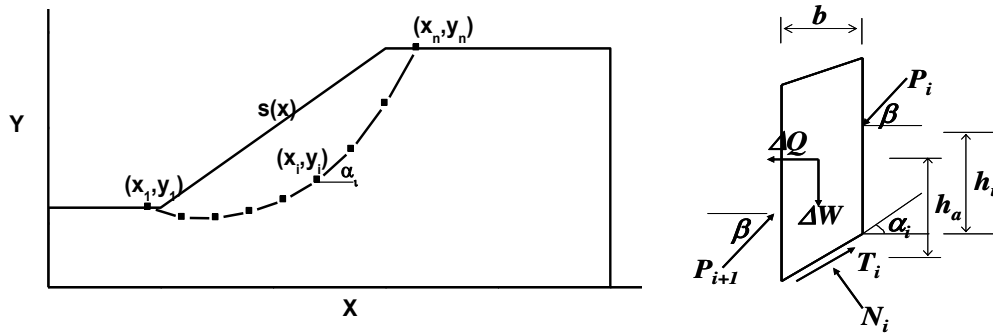
Fig.5. General cross section of slope (a) and forces acting on a typical slice (b)

A slip surface is represented by n nodal points with coordinates (x_1, y_1), (x_2, y_2), …,(x_n, y_n), respectively in the x-y plane (Fig. 5(a)). In order to minimize the number of variables, any two contiguous nodal points keep the same horizontal distance, which means

$$x_i = x_{i-1} + (x_n - x_1)/(n-1) \quad \text{for } i = 2, n-1$$
(19)

The abscissas of all nodal points should be enclosed within x_{min} and x_{max}, or mathematically

$$x_{min} \le x_i \le x_{max} \qquad \text{for } i = 1, n$$
(20)

Also, y_1 and y_n could be determined based on the topographic profile $s(x)$

$$y_i = s(x_i) \qquad \text{for } i = 1 \text{ and } i = n$$
(21)

As a result, a specific slip surface can be expressed mathematically by an n-element array

$$S = [x_1, y_2, y_3, ..., y_{n-1}, x_n]^T$$

(22)

The objective function locating the critical slip surface, which is defined as a surface with the minimum factor of safety among all the available ones, can be stated

$$\min F(S)$$

(23)

To make the slip surface kinematically admissible, these segments defined by any two contiguous nodal points are further assumed to be concave upward，which means that

$$\alpha_1 \le \alpha_2 \le \cdots \le \alpha_i \le \cdots \le \alpha_{n-1}$$

(24)

where α_i ,the inclination of segments, is limited between -45° and 60° to avoid computational divergence encountered in search for the safety factor [19].

Subsequently, the nodal points are connected by cubic-spline interpolation. Then the soil mass above the created slip surface is divided into many vertical slices. If there is a weak layer in the slope, it may intuitively be argued that the critical slip surface should extend along the weak layer for a substantial length of the slip surface. So if the abscissa of any slice base is lower than the weak layer, this slice base is adjusted to the weak layer.

The Spencer's method [20] is used to calculate the safety factor. The effect of inter-slice forces is included, by assuming the inter-slice force inclination angles of all slices to be equal. Both force and moment equilibrium is explicitly satisfied. Spencer's method is applicable to slip surface of any shapes, and considered as one of the accurate methods in the slope stability analysis. Fig. 5(b) shows the details of inter-slice forces for a typical slice.

The equations of force and momentum equilibrium can be respectively written as:

$$P_i = P_{i+1} + \frac{F\Delta W \sin\alpha_i - c'b\sec\alpha_i - \Delta W\cos\alpha_i \tan\varphi' + U_ib\sec\alpha_i \tan\varphi' + \Delta Q(F - \tan\varphi'\tan\alpha_i)\cos\alpha_i}{\sin(\beta - \alpha_i)\tan\varphi' - F\cos(\beta - \alpha_i)}$$

(25)

$$h_i = \frac{P_{i+1}}{P_i}h_{i+1} - \frac{P_{i+1}}{P_i}\frac{b}{2}\tan\alpha_i + \frac{b}{2}\tan\beta + \frac{P_{i+1}}{P_i}\frac{b}{2}\tan\beta - \frac{\Delta Qh_a}{P_i\cos\beta} - \frac{b}{2}\tan\alpha_i$$

(26)

where F is the factor of safety. P_i and P_{i+1} are the right and the left inter-slice force, respectively. N_i and U_i are the total normal force and the pore water pressure on the slice base, respectively. ΔW is the weight of slice and ΔQ is the horizontal force of slice. α_i is the angle between the slice base and the horizontal line. β is the inclination angle of inter-slice force. h_i and h_a are the height of force P_i and the center of the slice, respectively. b is the width of the slice.

An example is of a homogeneous slope (Fig. 6) with $\gamma = 17.64kN/m^3$, $\varphi' = 10°$ and $c' = 9.8kPa$. Yamagami and Ueta [21] utilized nonlinear programming methods, which are the DFP method, the BFGS method, the method of conjugate directions by Powell and simplex method, to locate the critical slip surfaces and the Morgenstern and Price method to calculate the factor of safety. Also Greco [22] used the Spencer's method in combination with a pattern search and Monte Carlo for the same problem. The comparison of the current results with those obtained by different researchers is summarized in Table 1.

Tab.1. Minimum safety factor given by minimization procedures for Example

Method	(a) Yamagami and Ueta (1988)				(b) Greco (1996)		(c) This Study
	BFGS	DFP	Powell	Simplex	Pattern search	Monte Carlo	Genetic algorithm
Range of safety factor	1.338	1.338	1.338	1.339-1.348	1.326–1.330	1.327–1.333	1.324 (line) 1.321 (spline)

It shows that when the slip surface is connected by spline curve, a better result can be reached. When the number of nodal points ranges from 4 to 8, the difference of the minimum safety factor is 0.009 for spline curve but 0.046

for straight line. Comparison of the geometry of the critical slip surfaces (Fig. 6) indicates that 4 nodal points connected by spline curve can generate similar critical slip surface to 13 nodal points connected by straight lines [22].
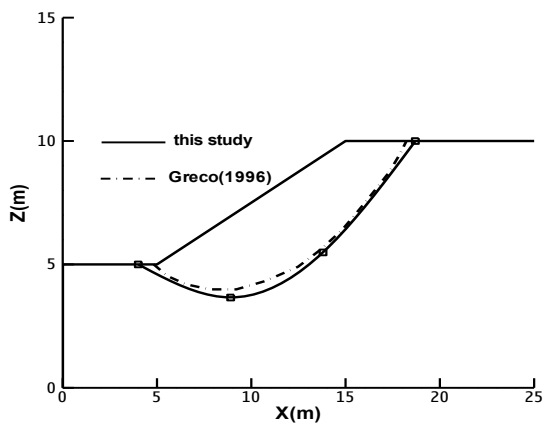
Fig.6. Cross section of slope of Example. The solid line represents the critical slip surface of this study, and the broken line is the solution given by Greco(1996)
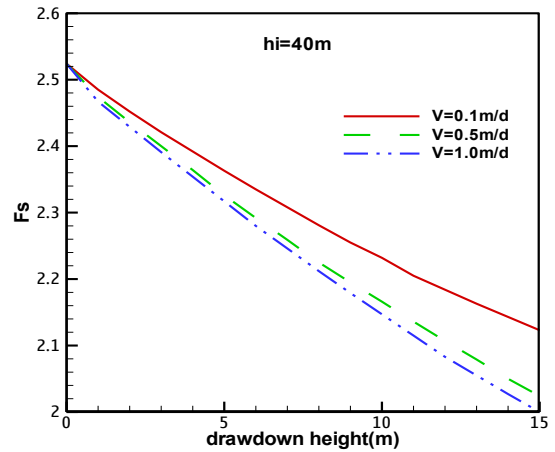
Fig.7. The variation of safety factor of slope with the drawdown velocity of water level

4. Effects of water seepage on slope stability

4.1. The effect of water level drawdown on slope stability

In section 2.2, an analytical solution of the linearized Boussinesq equation was developed for one-dimensional groundwater flow in unconfined aquifer. Based on the analytical solution, the stability of slope can be conveniently analyzed by using the stability analysis model. Based on the model shown in Fig. 2, we studied the effect of drawdown velocity of water level on the stability of slope. The results are shown in Fig. 7. Obviously, the faster the reservoir water level dropped down, the more the safety factor of slope reduced. It means the drawdown velocity of water level is a key factor of affecting the stability of slope. The greater drawdown velocity of water level would reduce the stability of slopes.
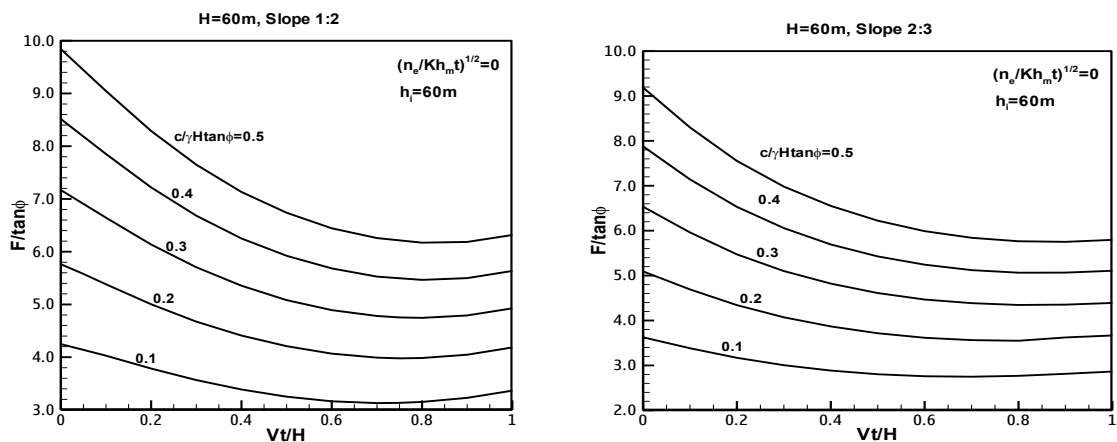
Fig. 8. Stability charts subjected to water level drawdown

By using the method to calculate the safety factor of slope needs a complex iteration calculating process. For convenient practical use, a series of stability charts subjected to water level drawdown are presented by establishing the function relationship of two nondimensional parameters of $F/\tan\varphi$ and $c_d/(\gamma H \tan\varphi_d)$ (see Fig. 8). And the safety factors can be obtained from the charts without the need for iteration.

4.2. Case Study

4.2.1. Brief introduction of Huayuan landslide

Huayuan landslide is located in Wanzhou District, Chongqing of China. The landslide occurred on the bank of Three Gorges Reservoir, with a length of about 380 m, a maximum width of 360 m, an average thickness of 18 m and a total volume of about 2470000 m³. Fig. 9 shows the cross section of the landslide. Based on some test results, the unit weight and strength parameters adopted in the limit equilibrium analyses are shown as: γ =20kN/m³, c =15kPa, ϕ =16°. Considering the effect of the matrix suction on shear strength, φ^b =13° and k_{sat} =1.0m/d.
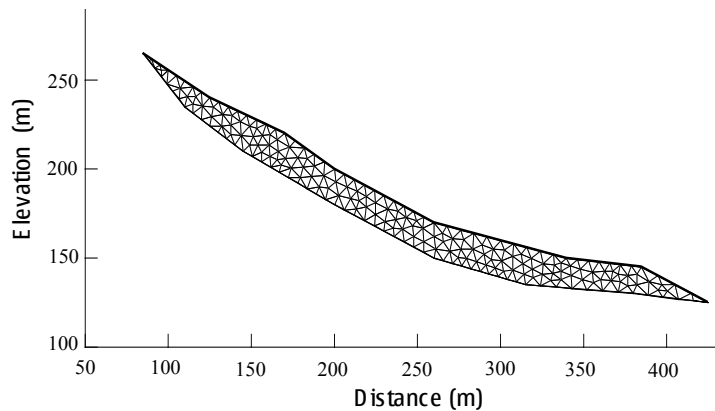
Fig. 9. Cross section of Huayuan landslide, which locates in Wanzhou District, Chongqing of China

4.2.2. Rainfall records and The process of water level for Three Gorges Reservoir operation

To investigate the effects of rainfall and Three Gorges Reservoir operation on the stability of the slope, the rainfall records collected by Fengjie monitoring station in 1998 and the water level process for reservoir operation are used. The rainfall records in 1998 is shown in Fig. 10, and the water level process of reservoir is shown in Fig. 11.
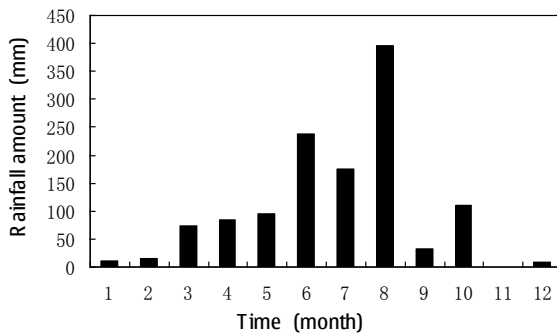
Fig.10. Monthly rainfall amount in 1998.
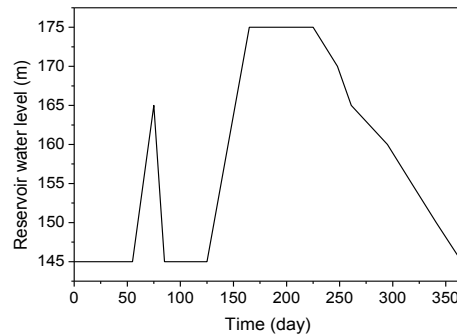
Fig.11. water level process for Three Gorges Reservoir operation

4.2.3. Numerical results

The saturated-unsaturated seepage model is applied to calculate the transient pore water pressure field in the slope caused by the rainfall and water level fluctuation. And the limit equilibrium method is employed to analyze the stability of slope. In order to examine the influences of rainfall and water level fluctuation on the slope stability, we firstly simulated the change process of the safety factor of slope caused by rainfall and water level fluctuation, respectively. Then we further calculated the development of slope safety factor under the joint action of rainfall and the water level fluctuation of reservoir. The simulated results are shown in Fig. 12.
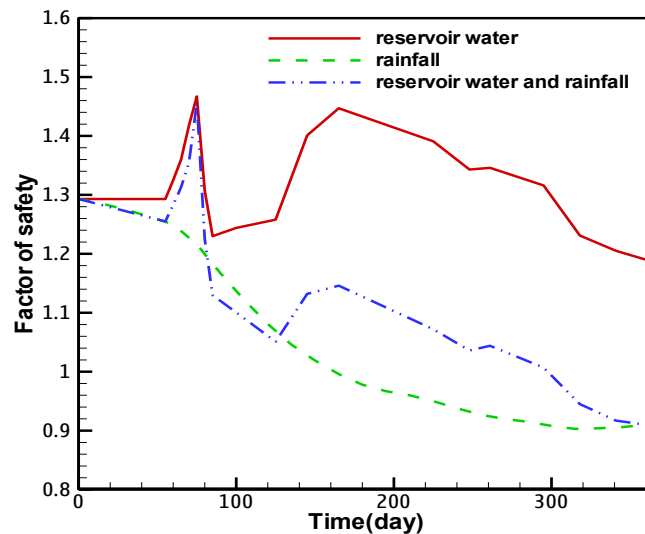
Fig. 12. Development of the safety factor caused by the joint action of rainfall and the water level fluctuation

The simulated results show that both rainfall and water level fluctuation of reservoir may cause the reduction of slope stability. The main reason leading to the reduction of slope stability is the increase of the total soil weight and the slight improvements of pore pressure in slip surface caused by rainfall infiltration and water level fluctuation. Especially, the continual rainfall leads to a continued reduction of safety factor of slope. The influence of water level fluctuation on the slope stability is complex, and the safety factor of slope will fluctuates with the reservoir water fluctuates. Under the joint action of both rainfall and water fluctuation, the safety factor of this landslide would have an observable decrease, and the slope is likely to occur instability. Moreover, the analysis above reveals that seepage caused by rainfall and water level fluctuation play a significant role on the stability of slopes.

5. Summary and Conclusions

With the finite element method and the limit equilibrium method, a coupling model of water-seepage and stability analysis has been developed. This model is able availably reflect the variations in pore pressure field in slopes, dead weight of soil, and the softening of soil strength caused by water seepage.

A combination of spline curves and genetic algorithm is used to locate the critical slip surface for slope stability calculations. When the slip surface is defined by spline curves, fewer nodal points are needed to reach the same accuracy, and to generate rational slip surfaces.

A new analytical solution of the linearized Boussinesq equation was developed for one-dimensional groundwater flow in unconfined aquifer. A series of stability charts subjected to water level drawdown are presented for convenient practical use, and the safety factors can be obtained from the charts without the need for iteration.

As case study, an actual landslide was studied to analyze the effects of rainfall and water level fluctuation on the seepage field and the slope stability. The results show that rainfall infiltration and the variation of water level can tremendously influence the stability of slope.

Acknowledgements

References

[1]   Iverson RM. Landslide triggering by rain infiltration. *Water Resour. Res.*, 2000, 36(7): 1897-1910.
[2]   Xu ZM, Huang RR, Fan ZG. Water-rock interaction in process of landslide preparing and triggering. *J. Nat. Disast.*, 2005, 14(1): 1-9 (in Chinese).
[3]   Sun JP, Liu QQ, Li JC. Effects of Rainfall Infiltration on the Stability of Soil Slopes. *Proceeding of the Fifth International Conference on Fluid Mechanics*, Shanghai, China, 2007, p. 459-462.
[4]   Ng CWW, Shi Q. A numerical investigation of the stability of unsaturated soil slopes subjected to transient seepage. *Computers and Geotechnics*, 1998, 22(1): 1-28.
[5]   Rahardjo H, Li XW, Toll DG, et al. The effect of antecedent rainfall on slope stability. *Geotech. Geol. Eng.*, 2001, 19: 371-399.
[6]   Tsaparas I, Rahardjo H, Toll DG, et al. Controlling parameters for rainfall-induced landslides. *Comput. Geotech.*, 2002, 29: 1-27.
[7]   Fan P, Liu QQ, Li JC, Sun JP. Numerical simulations of the infiltration of rain on the crack slope. *Sciences in China, Ser. E*, 2005, 48(Supp.): 107-120.
[8]   Sun JP, Liu QQ, Li JC, An Y. Effects of rainfall infiltration on deep slope failure. *Sciences in China –Physics Mechanics & Astronomy*, 2009, 52(1): 108-114.
[9]   Van Asch Th WJ, Buma J, Van Beek LPH. A view on some hydrological triggering systems in landslides. *Geomorphology*, 1999, 30: 25-32.
[10]   Yao HL, Zheng SQ, Chen SY. Analysis on the slope stability of expansive soils considering cracks and infiltration of rain. *Chin. J. Geotech. Eng.*, 2001, 23(5): 606-609 (in Chinese).
[11]   Yuan JP, Yin ZZ. Numerical model and simulation of expansive soils slope infiltration considered fissures. *Rock soil Mech.*, 2004, 25(10): 1581-1586 (in Chinese).
[12]   Fan HG, Liu QQ, An Y. Effects of Fracture Seepage on the Stability of Landslide during Reservoir Water Level Fluctuation. *Disaster Advances*, 2010, 3(4): 306-308.
[13]   Celia MA, Bouloutas ET. A general mass-conservative numerical solution for the unsaturated flow equation. *Water Resour. Res.*, 1990, 26(7): 1483-1496.
[14]   Rathfelder K, Abriola LM. Mass conservative numerical solutions of the head-based Richards equation. *Water Resour. Res.*, 1994, 30(9): 2579-2586.
[15]   Wu MX, Gao LS. Saturated-unsaturated unsteady seepage numerical analysis. *J Hydr. Eng.*, 1999, 12: 38-42(in Chinese).
[16]   Parlange JY, Stagnitti F, Starr JL, Braddock RD. Free-surface flow in porous media and periodic solution of the shallow-flow approximation. *J. Hydrol.*, 1984, 70: 251-263.
[17]   Sun JP, Li JC, Liu QQ, Zhang HQ. Approximate engineering solution for predicting groundwater table variation during reservoir drawdown on the basis of the Boussinesq equation. *J. Hydrol. Eng.*, 2011, 16(10): 791-797.
[18]   Sun JP, Li JC, Liu QQ. Search for Critical Slip Surface in Slope Stability Analysis by Spline-based GA Method. *J. Geotech. Geoenviron.*, 2008, 134(2), 252-256.
[19]   Malkawai AIH, Hassan WF, Sarma SK. Global search method for locating general slip surface using Monte Carlo techniques. *J. Geotech. Geoenviron.*, 2001, 127 (8): 688–698.
[20]   Spencer E. A method of analysis of the stability of embankments assuming parallel interslice forces. *Geotechnique*, 1967, 17(1): 11–26.
[21]   Yamagami T, Ueta Y. Search for noncircular slip surfaces by the Morgenstern-Price method. *Proc., 6th Int. Conf. Number. Methods in Geomechanics*, 1988, p.1219–1223.
[22]   Greco VR. Efficient Monte Carlo technique for locating critical slip surface. *J. Geotech. Engr. -ASCE*, 1996, 122(7): 517–525.